Computer Simulation of an Entangled Micronetwork: Analysis of Junction Fluctuations in Uniaxial Extension

D. B. Adolf* and J. G. Curro

Sandia National Laboratories, Albuquerque, New Mexico 87185. *Received October 14, 1986*

ABSTRACT: Computer simulations were performed on entangled micronetworks in uniaxial extension. Network chains of 41 beads were studied with various entanglement spacings. The mean-square fluctuations of the free network junction were computed as a function of strain in the directions parallel and perpendicular to the strain direction. The computer simulation results compare favorably with the predictions from the Ronca–Allegra and Flory–Erman constrained junction theories. The κ parameter in the Flory theory, which measures the strength of the entanglement, was found to have an approximate linear dependence on the network chain length, in contrast to earlier predictions.

Introduction

The practical importance of elastomers has generated a great number of experimental and theoretical studies for over 5 decades. While significant strides were made at an early stage, a complete understanding of the molecular physics has yet to be achieved. This is not surprising considering the complex interchain interactions in these dense, cross-linked systems. The purpose of the present investigation is to gain a further understanding of the elasticity of polymer networks through computer simulation of micronetworks in uniaxial extension.

The principal assumption made in early rubber elasticity theories was that the free energy change with deformation is entirely due to entropy change.[1] Experimental studies have demonstrated that this assumption is reasonable in that energetic contributions usually amount to less than 20% of the total free energy change.[1] This accounts for the vastly different elastic behaviors of polymer networks and crystalline solids, in which the elastic free energy is dominated by energetic contributions. In order to construct a molecular theory for the entropy change in a polymer network upon deformation, the earliest theories assumed that a network is composed of freely interpenetrating, Gaussian chains (no excluded volume or entanglement effects).

One additional assumption had to be made relating the macroscopic deformation of the sample to the microscopic deformation of the network chains. The simplest assumption is that this deformation is affine;[2] that is, each end-to-end vector deforms proportionally to the macroscopic strain. This implies that the network junctions are embedded in a continuum and do not fluctuate. Subsequent to the affine model, James and Guth[3] developed the so-called phantom network model. In this model, there are "fixed junctions" that move affinely and "free junctions" that can fluctuate. The resultant behavior for each end-to-end vector is, therefore, nonaffine. Recent neutron scattering experiments on partially deuteriated networks suggest that neither the affine model nor the phantom model are entirely correct.[4]

The element missing from these early theories is the effect of entanglements. Entanglements act as topological constraints and profoundly affect the way in which individual polymer chains move in response to a macroscopically imposed strain. Recent theories have attempted to address the effect of entanglements. These theories fall into two major categories based on their approach to the entanglement problem. The first set of theories[5–7] tries to explicitly account for neighboring network chains becoming entangled. This is accomplished with topological invariants,[5] slip-links,[6] and tubes.[7] The second set of theories,[8–10] sometimes called constrained junction models, assumes that the entanglements modify the strain dependence of the end-to-end vector distribution function. In other words, the entanglements affect only the magnitude of the network junction fluctuations.

This second approach is mathematically more tractable but assumes that junction fluctuations along a given axis are suppressed by entanglements, are dependent only on the extension ratio along that axis, and increase with increasing extension ratio. In the Flory theory, the mean-square magnitude of the junction fluctuations along the i-th principal axis is dependent on the extension ratio along that axis, λ_i, and is given by[9]

$$\langle \delta x_i^2 \rangle_F = \langle \delta x_i^2 \rangle_{PN}/(1 + \kappa/\lambda_i^2) \qquad i = 1, 3 \qquad (1)$$

where $\langle \delta x_i^2 \rangle_{PN}$ is the mean-square fluctuation magnitude along the i-th principal axis for the phantom network model, which is independent of strain, and κ is a material constant measuring the severity of the entanglement constraints on the network junction points. The Ronca–Allegra[8] and Flory–Erman[10] theories yield relationships similar to eq 1. In principle, the magnitude of the junction fluctuations can also be calculated for the Edwards' theories.[5–7]

In the computer simulation approach presented here, we will focus our attention on the effect of entanglements on the junction fluctuations. In order to make the calculation feasible, we performed our calculations on a rank one micronetwork having a functionality of 3. In this micronetwork, shown in Figure 1, we take the three chain ends to be fixed (as are the fixed junctions in the phantom network theory) and we investigate the statistics associated with the branch point or free junction. This problem, in the absence of entanglements, is a special case of the James–Guth theory and was solved exactly for Gaussian chains by Graessley.[11,12] The mean-square junction fluctuations were found to be isotropic, independent of deformation, and equal to $N/9$, where N is the number of segments between junctions. In our simulations, we can directly compute the mean-square fluctuations of the free junction with and without entanglements. Thus, we can directly test the assumptions that enter into the various rubber elasticity models, which is very difficult to do experimentally.

Simulation

We have simulated a rank one micronetwork on a CDC Cyber 180/855. Three chains, each of 41 beads, were placed on a cubic lattice. With the assumption that each simulation segment corresponds to at least five real monomers (based on a value for the characteristic ratio[13]), the simulation chains should mimic real chains with degree of polymerization of at least 200. Exact calculations on unentangled micronetworks of 40-unit, freely rotating chains show Gaussian behavior (deviations from phantom micronetwork theory[11,12] of less than 5%) for extension

0024-9297/87/2220-1646$01.50/0

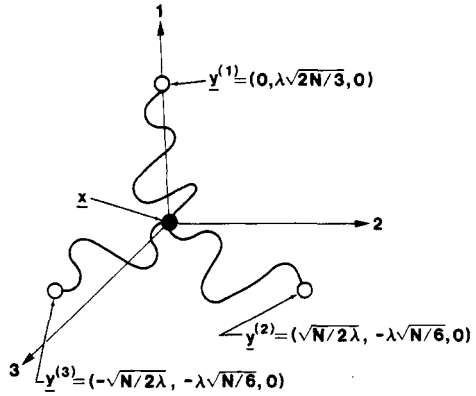

Figure 1. Rank-one, trifunctional micronetwork with three fixed chain ends ($y^{(1)}$, $y^{(2)}$, $y^{(3)}$) lying in the x_1–x_2 plane and one fluctuating junction point (x).

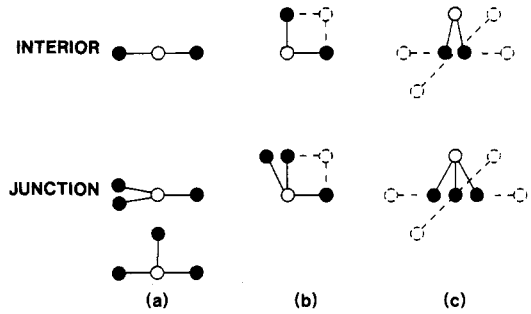

Figure 2. Possible configurations for interior and junction beads. No movement is allowed for configuration of type a. Configurations of type b must move as shown, and those of type c have four placement options.

ratios less than 3.[14] To avoid non-Gaussian effects in our entangled network simulations, we kept the extension ratio less than 2.1. Micronetwork calculations show that these 40-segment chains exhibit Gaussian statistics for uniaxial extension ratios of less than 2.5.[14]

Different chain configurations were sampled with the dynamic scheme of Evans and Edwards[15,16] (a modification of Verdier–Stockmayer dynamics[17]). In this scheme, there is no excluded volume, as would be expected for unswollen networks, and interior beads and junctions move as shown in Figure 2. Although we are only interested in equilibrium properties, it is interesting to note that this model yields Rouse dynamics[18] for linear chains with 5–50 beads[15] and for three-arm stars with 4–22 beads per arm.[16]

Entanglements were simulated by again following the dynamic scheme of Evans and Edwards. An obstacle net with a mesh spacing c times the network chain lattice spacing was introduced. Bead moves shown in Figure 2 are forbidden if they require the chain to pass through a segment of the obstacle net. As noted by Evans and Edwards, it is important that the obstacle net not overlap the chain lattice so that excluded volume is again avoided (see Figure 3). This entangled model yields "reptation dynamics"[19] for linear chains of 5–50 beads with $c = 2$[15] and "primitive path retracing dynamics"[20] for three-arm stars of 4–22 beads per arm with $c = 1$.[16] We chose the entanglement spacing, c, to be 2 and 4 for our network simulations.

The starting positions for the three fixed-chain ends in the unstrained, unentangled state were determined by assuming Gaussian chain statistics. This results in the mean-square end-to-end distance of chain α being given by

$$\langle R^{(\alpha)2}\rangle = \sum_{i=1}^{3}[(y_i^{(\alpha)} - \langle x_i\rangle)^2 + \langle \delta x_i^2\rangle] = N \qquad (2)$$

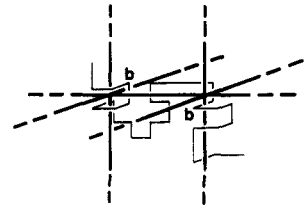

Figure 3. Typical configuration of one cubic lattice chain embedded in an entanglement obstacle net. Note that the obstacle net and chain lattice do not overlap. The beads, b, although in configurations where movement is allowed, cannot move due to the obstacle net.

where x_i is the i-th component of the position of the network junction, $y_i^{(\alpha)}$ is the i-th component of the fixed end of chain α (see Figure 1), N is the number of segments per chain, and the segment length is taken to be unity. $\langle \delta x_i^2\rangle$ is the mean-square fluctuation of the i-th component of the network junction defined as

$$\langle \delta x_i^2\rangle = \langle x_i - \langle x_i\rangle\rangle^2 = \langle x_i^2\rangle - \langle x_i\rangle^2 \qquad (3)$$

As shown by Graessley,[11] $\langle \delta x_i^2\rangle = N/9$ for a trifunctional, rank-one micronetwork, and

$$\langle x_i\rangle = (1/3)\sum_{i=1}^{3} y_i^{(\alpha)} \qquad (4)$$

We define our coordinate system such that $\langle x_i\rangle$ is zero ($i = 1, 2, 3$) and the three chains lie in the x_1–x_2 plane with chain 1 along the x_2 axis (see Figure 1). The fixed chain ends, for the undeformed state, can then be shown to be located at

$$y^{(1)} = (0, (2N/3)^{1/2}, 0)$$
$$y^{(2)} = ((N/2)^{1/2}, -(N/6)^{1/2}, 0)$$
$$y^{(3)} = (-(N/2)^{1/2}, -(N/6)^{1/2}, 0) \qquad (5)$$

For ease of comparison, the entangled chains also have these fixed-end coordinates.

The chains themselves are initially laid down in an arbitrary fashion connecting the fixed end and network junction. Calculation of simulation averages is delayed by a specified amount in order to minimize the effect of these initial configurations. When a uniaxial strain is "applied", the fixed chain ends and the entanglement net are assumed to deform affinely (while maintaining constant volume), and a new chain is laid down connecting the fixed end and network junction followed by another calculation delay. Note that the entanglement net can undergo exact affine deformation, whereas the fixed-chain ends can only approximately follow the prescribed affine deformation. This is due to the requirements of constant segment length and number of beads per chain.

Except for the mentioned initial delay, the mean junction position $\langle x_i\rangle$, the mean-square junction position $\langle x_i^2\rangle$, and the cross terms $\langle x_i x_j\rangle$ ($i \neq j$) are calculated after every bead move. From simulations on unentangled micronetworks involving 10 million steps, we have determined that approximately 2 million steps are required to reproduce the exact values for the junction averages (within the equilibrium fluctuations). For entangled micronetworks, we also need to sample different initial configurations since not all configurations are available due to the immovable obstacle net. Simulations on six different entanglement topologies showed that the junction fluctuation averages are not extremely sensitive to the initial configuration (an upper bound on the statistical deviation of 10%).[21]

From the three simulation averages given above, we have calculated the following physically important averages: the

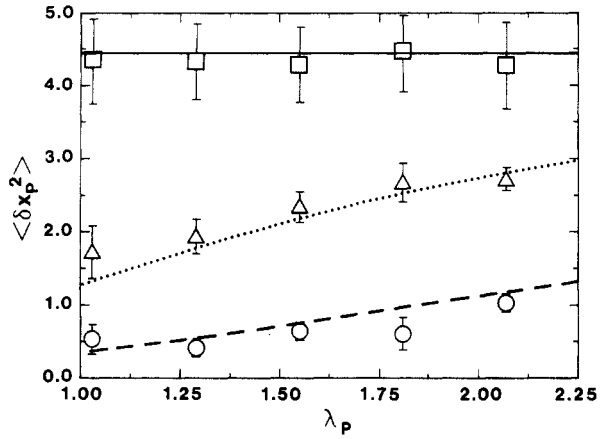

Figure 4. Mean-square junction fluctuations parallel to the uniaxial extension ratio plotted vs. extension ratio for simulation runs with different entanglement spacings: (□) $c = \infty$ (unentangled); (△) $c = 4$; (○) $c = 2$. Lines from the theoretical predictions for a phantom network (—) and for the Flory constrained junction model with $\kappa = 2.5$ (···) and 12 (– – –).

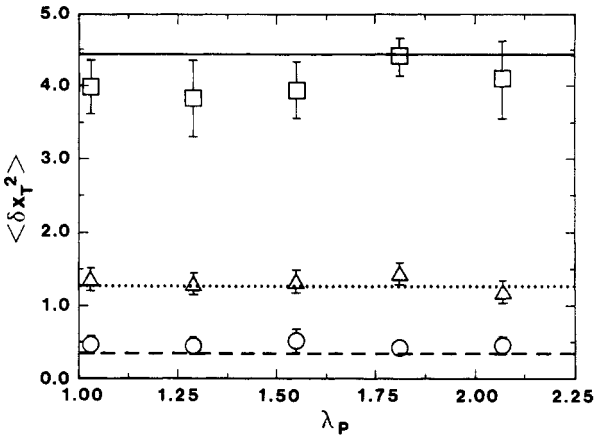

Figure 5. Mean-square junction fluctuations perpendicular to the uniaxial extension ratio plotted vs. extension ratio for simulation runs with different entanglement spacings: (□) $c = \infty$ (unentangled); (△) $c = 4$; (○) $c = 2$. Lines from the theoretical predictions for a phantom network (—) and for the Flory constrained junction model with $\kappa = 2.5$ (···) and 12 (– – –).

mean junction fluctuaions $\langle \delta x_i \rangle = \langle x_i - \langle x_i \rangle \rangle$, the mean-square magnitude of the junction fluctuations $\langle \delta x_i^2 \rangle$,[11] the junction fluctuation cross terms $\langle \delta x_i \delta x_j \rangle$ $(i \neq j)$, and the mean-square end-to-end distance for chain α in the i-th direction $\langle R_i^{(\alpha)2} \rangle$. These averages are compared with theory in the next section.

Results and Discussion

We will first examine the junction fluctuations parallel to the direction of extension, $\langle \delta x_P^2 \rangle$. For no entanglements (i.e., $c = \infty$), the simulation should mimic a phantom micronetwork for which $\langle \delta x_P^2 \rangle$ is independent of extension ratio and equal to $N/9 = 4.44$. In Figure 4, we see that, within the uncertainty limits, the simulation fluctuations are constant and equal to the phantom micronetwork value. As the entanglement spacing decreases, the Flory constrained junction theory predicts that the fluctuations should become suppressed. The suppression, however, should weaken as the entanglements move farther apart with the increase in extension ratio. Figure 4 shows that the simulation not only qualitatively follows this trend but quantitatively follows the Flory prediction of eq 1. For simulation entanglement spacings of 2 and 4, Flory parameters (κ) of 12 and 2.5, respectively, were used to compare theory and experiment. Again, κ is a measure of the severity of the entanglement constraints in the Flory theory, so larger values of κ naturally correspond to smaller simulation entanglement spacings.

We will now examine the junction fluctuations perpendicular to the direction of extension. For no entanglements, the transverse fluctuations $\langle \delta x_T^2 \rangle = (\langle \delta x_2^2 \rangle + \langle \delta x_3^2 \rangle)/2$, should be constant and equal to 4.44, which is seen in Figure 5. Simulation results show more scatter in this case, but tend to agree with the phantom micronetwork theory. As the entanglement spacing is decreased, the fluctuations should be suppressed. This fluctuation suppression should become stronger with increasing extension ratio, since we are trying to simulate uniaxial extension where there is a compression of the entanglement net perpendicular to the extension caused by the constant density constraint (i.e., if $\lambda_P = \lambda$, then $\lambda_T = \lambda^{-1/2}$). However, as described previously, the fixed-chain ends can occupy only the nodes of a cubic lattice and, therefore, cannot exactly reproduce the requested extension ratios. We actually find that a transverse extension ratio of unity throughout the range $1 \geq \lambda_p \geq 2.25$ is the best approximation to constant volume that we can achieve subject to this lattice constraint. In this case, $\langle \delta x_T^2 \rangle$ should remain constant at the $\lambda_p = 1$ values. Figure 5 shows that the simulation fluctuations for entanglement spacings of 2 and 4 are constant and equal in magnitude to the Flory predictions with the same values of κ (12 and 2.5, respectively) used previously. These κ values best fit the combined parallel and transverse fluctuation data.

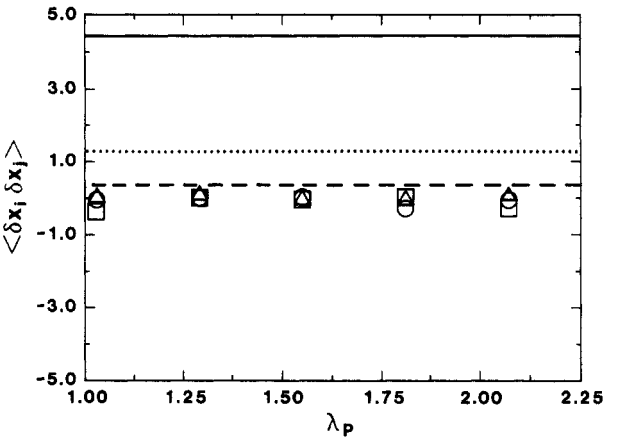

Figure 6. Junction fluctuation cross terms $(i \neq j)$ plotted vs. the uniaxial extension ratio for simulation runs with different entanglement spacings: (□) $c = \infty$ (unentangled); (△) $c = 4$, (○) $c = 2$. Lines show the magnitude of the mean-square junction fluctuations at $\lambda_p = 1$ for the phantom network (—) and the Flory constrained junction model with $\kappa = 2.5$ (···) and 12 (– – –).

Figures 4 and 5 indicate that the constrained junction model of Flory *quantitatively* predicts the magnitude of the junction fluctuations parallel and perpendicular to the direction of extension. We can also test the Flory assumption that the parallel and transverse fluctuations are independent by examining the fluctuation cross terms, $\langle \delta x_i \delta x_j \rangle$, where $i \neq j$. These cross terms should vanish if the parallel and transverse fluctuations are uncorrelated. In Figure 6, we see that these cross terms are indeed negligible in comparison to the mean-square fluctuations for the phantom micronetwork and Flory theories.

The mean-square end-to-end distance for chain α in the i-th direction can be related to the junction fluctuations by

$$\langle R_i^{(\alpha)2} \rangle = y_i^{(k)2} - 2\langle x_i \rangle y_i^{(k)} + \langle x_i \rangle^2 + \langle \delta x_i^2 \rangle \qquad (6)$$

The average of $\langle R_i^{(\alpha)2} \rangle$ over all three chains is expressed

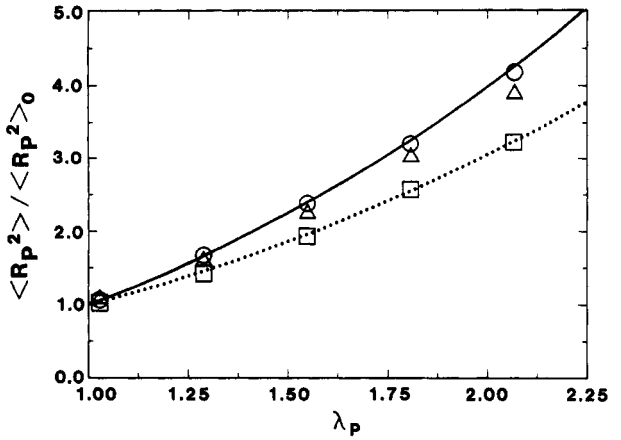

Figure 7. Average over all three chains of the mean-square end-to-end distance parallel to the uniaxial extension ratio plotted vs. extension ratio for simulation runs with different entanglement spacings: (□) $c = \infty$ (unentangled); (△) $c = 4$; (○) $c = 2$. Lines from the theoretical predictions for the affine model (—) and the phantom network (···).

as $\langle R_i^2 \rangle$ and is plotted in Figure 7 for the affine and phantom micronetwork models, which represent the limiting cases. The simulation results for infinite entanglement spacing agree well with the phantom micronetwork theory, and, as c is decreased, the simulation results creep closer to the affine model, as expected. This trend was observed experimentally by Yu et al.[4] on trifunctional polyisoprene networks using neutron scattering. However, it is apparent that the assumptions of the Flory theory are not easily confirmed by this type of plot since the difference between the two limits is not great. Much more constrast is seen by examining the junction fluctuations directly. Experimentally, the error associated with neutron scattering from networks with isolated deuteriated chains is probably too large to accurately verify the molecular assumptions made in the Flory theory, making this type of computer simulation one of the few methods by which to examine directly the molecular assumptions in the Flory theory.

Finally, we examined the dependence of the Flory parameter, κ, on simulation variables such as chain length, N, and entanglement spacing, c. If the simulation chains are Gaussian, κ should only be a function of N/N_e, where $N_e = c^2$. That is, a chain of 40 segments in an obstacle net with an entanglement spacing of 2 ($N_e = 4$) should be equivalent to a 90-unit chain in a net with $c = 3$ ($N_e = 9$). Erman and Flory suggested that $\kappa \sim N^{1/2}$ by examining chain interpenetration.[22] The validity of eq 1 is independent of this relationship. In figure 8, we have plotted the best fit κ from the simulation runs mentioned above and from a run for a 21-bead chain with entanglement spacing of 2 ($N/N_e = 5$) against N/N_e. (It should be noted that the 21-bead chain showed deviations from the Flory predictions for extension ratios greater than 2, which are probably due to non-Gaussian effects.[14] Therefore, only the $\lambda = 1$ data point was used to extract the value of κ.) There are only three points and much scatter, but the relationship is definitely not square root as predicted by the interpenetration theory. It may be linear. Experimental force–extension results also show much scatter but seem to indicate that the square root dependence is too weak (see Figure 9).[23]

We now give a scaling argument showing that the exponent for a power-law dependence of κ on N/N_e (i.e., $\kappa \sim (N/N_e)^\gamma$) has upper and lower bounds. The lower bound is easily found by noticing that κ must be an increasing function of N/N_e. Therefore, the exponent γ

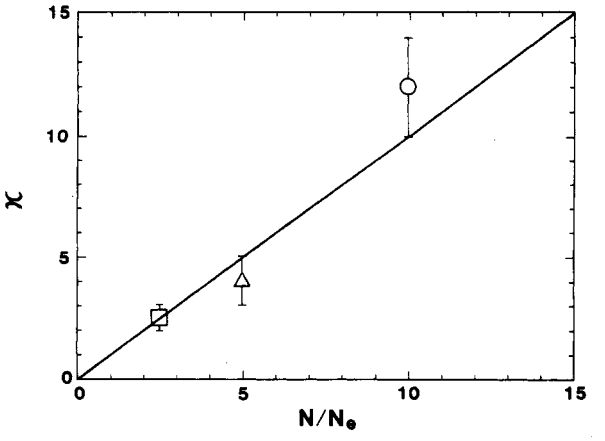

Figure 8. κ parameter from the Flory constrained junction model plotted vs. the ratio of the number of beads per chain, N, to the number of beads needed for a random walk between obstacles, $N_e = c^2$. Points from simulation runs with $N = 40$ and $N_e = 16$ (□), $N = 20$ and $N_e = 4$ (△), and $N = 40$ and $N_e = 4$ (○).

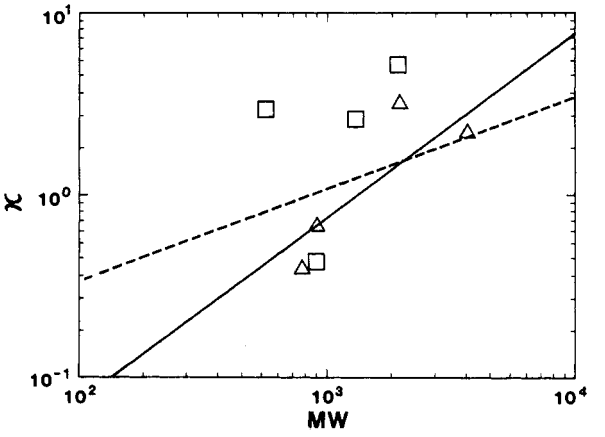

Figure 9. Double-logarithmic plot of the κ parameter from the Flory constrained junction model vs. the molecular weight between cross-links. Data are taken from ref 22 for unswollen poly(oxypropylene) (△) and poly(ε-caprolactone) (□). Solid line has slope of 1. Dotted line has slope of $^1/_2$.

must obey the inequality $\gamma \geq 0$. To obtain the upper bound, we incorporate the assumed power-law dependence of κ into eq 1. The junction fluctuations in the unstrained state ($\lambda_i = 1$) can then be expressed as

$$\langle \delta x_i^2 \rangle_F = \frac{\langle \delta x_i^2 \rangle_{PN}}{1 + \beta(N/N_e)^\gamma} \tag{7}$$

where β is a constant independent of N/N_e. The phantom network fluctuations, $\langle \delta x_i^2 \rangle_{PN}$, as stated previously, equal $N/9$ for a trifunctional, rank-one micronetwork[11] and, in general, for any network,[1] are proportional to N. In the limit as $N \to \infty$ (N_e fixed), $\beta(N/N_e)^\gamma \gg 1$ and we obtain

$$\lim_{N\to\infty} \langle \delta x_i^2 \rangle_F \sim \frac{N}{(N/N_e)^\gamma} \sim N^{1-\gamma} \tag{8}$$

The upper bound on the exponent γ is then found by claiming that the network junction fluctuations in eq 8 must not decrease as N increases. The exponent γ must, therefore, obey the inequality $\gamma \leq 1$. We see then that $0 \leq \gamma \leq 1$, which allows both the Erman–Flory theory ($\kappa \sim N^{1/2}$) and a linear relationship seen in our simulation. The two results are qualitatively different, however, in that the Erman–Flory result ($\gamma = {}^1/_2$) implies that the network junction fluctuations are unbounded as $N \to \infty$ whereas the simulation results ($\gamma = 1$) implies that the junction fluctuations remain bounded as $N \to \infty$.

Conclusions

We have examined the magnitude of the junction fluctuations in an entangled micronetwork with a computer simulation and have found that the Flory constrained junction theory quantitatively predicts the strain dependence of the fluctuations over the range of extension ratios investigated. The mean-square junction fluctuations along the three principal axes are also independent as predicted by theory. The sole parameter of the Flory theory, κ, does not seem to follow the predictions of a later, independent theory of Erman and Flory, which states that κ should be proportional to the square root of the network chain molecular weight. The computer simulation results show a stronger dependence on molecular weight. Not enough data have been collected, however, to conclude if this is representative of real networks or is caused by finite system size effects (i.e., short chains of low-rank micronetworks).

It should be emphasized that comparison of the results of this computer simulation with theory need not be confined to contrained junction models. For example, the junction fluctuations from the Edwards' theories,[5-7] if available, could also be compared. In addition, the fact that agreement between constrained junction theory and computer simulation was found for the junction fluctuations does not imply similar agreement for the free energy or equation of state. Future computer simulations of entangled micronetworks are planned to address the strain dependence of the free energy.

Acknowledgment. This work was performed at Sandia National Laboratories supported by the U.S. Department of Energy under Contract No. DE-AC04-76DP00789.

References and Notes

(1) Treloar, L. R. G. *The Physics of Rubber Elasticity*; Oxford University Press: London, 1958.
(2) Flory, P. J. *Principles of Polymer Chemistry*; Cornell University Press: Ithaca, NY, 1956.
(3) James, H. M.; Guth, E. *J. Chem. Phys.* **1943**, *11*, 455.
(4) (a) For a summary see: Ullman, R. In *Elastomers and Rubber Elasticity*; Mark, J. E., Lal, J., Ed.; American Chemical Society: Washington, D.C., 1982. (b) Yu, H.; Kitano, T.; Chung, Y. K.; Amis, E. J.; Chang, T.; Landry, M. R.; Wesson, J. A.; Han, C. C.; Lodge, T. P.; Glinka, C. J., submitted for publication.
(5) Deam, R. T.; Edwards, S. F. *Philos. Trans. R. Soc. London A* **1976**, *280*, 317.
(6) Ball, R. C.; Doi, M.; Edwards, S. F.; Warner, M. *Polymer* **1981**, *22*, 1010.
(7) Edwards, S. F.; Vilgis, Th. *Polymer* **1986**, *27*, 483.
(8) Ronca, G.; Allegra, G. *J. Chem. Phys.* **1975**, *63*, 4990.
(9) Flory, P. J. *J. Chem. Phys.* **1977**, *66*, 5720.
(10) Flory, P. J.; Erman, B. *Macromolecules* **1982**, *15*, 800.
(11) Graessley, W. W. *Macromolecules* **1975**, *8*, 186.
(12) Graessley, W. W. *Macromolecules* **1975**, *8*, 865.
(13) Flory, P. J. *Statistical Mechanics of Chain Molecules*; Interscience: New York, 1969.
(14) A more complete study of non-Gaussian effects is to be submitted for publication.
(15) Evans, K. E.; Edwards, S. F. *J. Chem. Soc., Faraday Trans. 2* **1981**, *77*, 1891.
(16) Needs, R. J.; Edwards, S. F. *Macromolecules* **1983**, *16*, 1492.
(17) Verdier, R. H.; Stockmayer, W. H. *J. Chem. Phys.* **1962**, *36*, 227.
(18) Bird, R. B.; Hassager, O.; Armstrong, R. C.; Curtiss, C. F. *Dynamics of Polymeric Liquids*; Wiley: New York, 1977; Vol. 2.
(19) Doi, M.; Edwards, S. F. *J. Chem. Soc., Faraday Trans. 2* **1978**, *74*, 1789.
(20) Pearson, D. S.; Helfand, E. *Macromolecules* **1984**, *17*, 888.
(21) It should be noted that, strictly speaking, the simulation should proceed by generating configurations in the unstrained state and then propagating these to the deformed state in order to preserve entanglement topologies. This is a much more difficult simulation scheme and should be equivalent to our procedure if we choose the appropriate weighting for deformed state initial configurations. We approximate this weighting as uniform which, we argue, should be reasonable in the range of extension ratios examined here. In addition, as stated in the text, calculated averages are fairly insensitive to entanglement topology; therefore, the exact choice for the weighting function is not crucial, and our simulation will provide fluctuation averages in agreement with an exact scheme.
(22) Erman, B.; Flory, P. J. *Macromolecules* **1982**, *15*, 806.
(23) Brotzman, R. W.; Mark, J. E. *Macromolecules* **1986**, *19*, 667.